Inorganic Chemistry

Article

pubs.acs.org/IC

Heterometallic Coordination Polymers Assembled from Trigonal Trinuclear Fe_2Ni-Pivalate Blocks and Polypyridine Spacers: Topological Diversity, Sorption, and Catalytic Properties

Svetlana A. Sotnik,[†] Ruslan A. Polunin,[†] Mikhail A. Kiskin,*[,‡] Alexander M. Kirillov,[§] Victoria N. Dorofeeva,[†,∥] Konstantin S. Gavrilenko,[∥,⊥] Igor L. Eremenko,[‡] Vladimir M. Novotortsev,[‡] and Sergey V. Kolotilov*[,†]

[†]L. V. Pisarzhevskii Institute of Physical Chemistry of the National Academy of Sciences of the Ukraine, Prospekt Nauki 31, Kiev 03028, Ukraine

[‡]N. S. Kurnakov Institute of General and Inorganic Chemistry, Russian Academy of Sciences, Leninsky Prosp. 31, 119991 GSP-1 Moscow, Russian Federation

[§]Centro de Química Estrutural, Complexo I, Instituto Superior Técnico, Universidade de Lisboa, Av. Rovisco Pais, 1049-001 Lisbon, Portugal

[∥]Research-And-Education ChemBioCenter, National Taras Shevchenko University of Kyiv, Chervonotkackaya str., 61, Kiev 03022, Ukraine

[⊥]Enamine Ltd., A. Matrosova str. 23, Kiev 01103, Ukraine

Supporting Information

ABSTRACT: Linkage of the trigonal complex $[Fe_2NiO(Piv)_6]$ (where Piv^- = pivalate) by a series of polypyridine ligands, namely, tris(4-pyridyl)triazine (L^2), 2,6-bis(3-pyridyl)-4-(4-pyridyl)pyridine (L^3), *N*-(bis-2,2-(4-pyridyloxymethyl)-3-(4-pyridyloxy)propyl))pyridone-4 (L^4), and 4-(*N*,*N*-diethylamino)phenyl-bis-2,6-(4-pyridyl)pyridine (L^5) resulted in the formation of novel coordination polymers $[Fe_2NiO(Piv)_6(L^2)]_n$ (**2**), $[Fe_2NiO(Piv)_6(L^3)]_n$ (**3**), $[Fe_2NiO(Piv)_6(L^4)]_n \cdot n$HPiv (**4**), and $[\{Fe_2NiO(Piv)_6\}_4\{L^5\}_6]_n \cdot 3n$DEF (**5**, where DEF is *N*,*N*-diethylformamide), which were crystallographically characterized. The topological analysis of **3**, **4**, and **5** disclosed the 3,3,4,4-connected 2D (**3**, **4**) or 3,4,4-connected 1D (**5**) underlying networks which, upon further simplification, gave rise to the uninodal 3-connected nets with the respective fes (**3**, **4**) or SP 1-periodic net (4,4)(0,2) (**5**) topologies, driven by the cluster $[Fe_2Ni(\mu_3\text{-}O)(\mu\text{-}Piv)_6]$ nodes and the polypyridine μ_3-$L^{3,4}$ or μ_2-L^5 blocks. The obtained topologies were compared with those identified in other closely related derivatives $[Fe_2NiO(Piv)_6(L^1)]_n$ (**1**) and $\{Fe_2NiO(Piv)_6\}_8\{L^6\}_{12}$ (**6**), where L^1 and L^6 are tris(4-pyridyl)pyridine and 4-(*N*,*N*-dimethylamino)phenyl-bis-2,6-(4-pyridyl)pyridine, respectively. It was shown that a key structure-driven role in defining the dimensionality and topology of the resulting coordination network is played by the type of polypyridine spacer. Compounds **2** and **3** possess a porous structure, as confirmed by the N_2 and H_2 sorption data at 78 K. Methanol and ethanol sorption by **2** was also studied indicating that the pores filled by these substrates did not induce any structural rearrangement of this sorbent. Additionally, porous coordination polymer **2** was also applied as a heterogeneous catalyst for the condensation of salicylaldehyde or 9-anthracenecarbaldehyde with malononitrile. The best activity of **2** was observed in the case of salicylaldehyde substrate, resulting in up to 88% conversion into 2-imino-2*H*-chromen-3-carbonitrile.

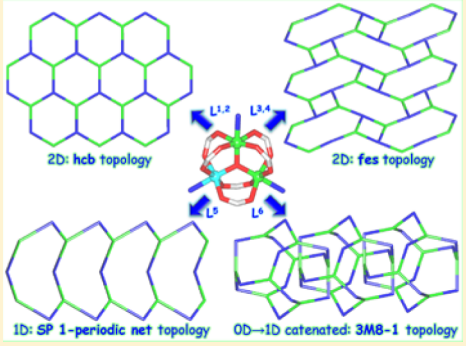

INTRODUCTION

Porous coordination polymers (PCPs) are considered as a basis for the creation of functional materials for sorption and separation processes,[1] catalysis,[2] luminescent,[3] or magnetic applications.[4] Due to the unique possibility of PCPs to combine several properties within one structure, such compounds have a recognized potential to become multifunctional materials.[1c,5] Sorption properties of PCPs are determined by their porosity that depends on the crystal structures of such compounds and the arrangement of structural elements. On the other hand, magnetic, catalytic, luminescent, and other properties of PCPs are determined by the composition and structure of metal-containing units. Despite numerous methods having been developed for the synthesis of PCPs, in the overwhelming majority of cases it is impossible to rationally predict the structure of the resulting compounds, since the same reagents can often lead to completely different products, depending on

Received: December 30, 2014
Published: May 8, 2015

DOI: 10.1021/ic503061z
Inorg. Chem. 2015, 54, 5169−5181

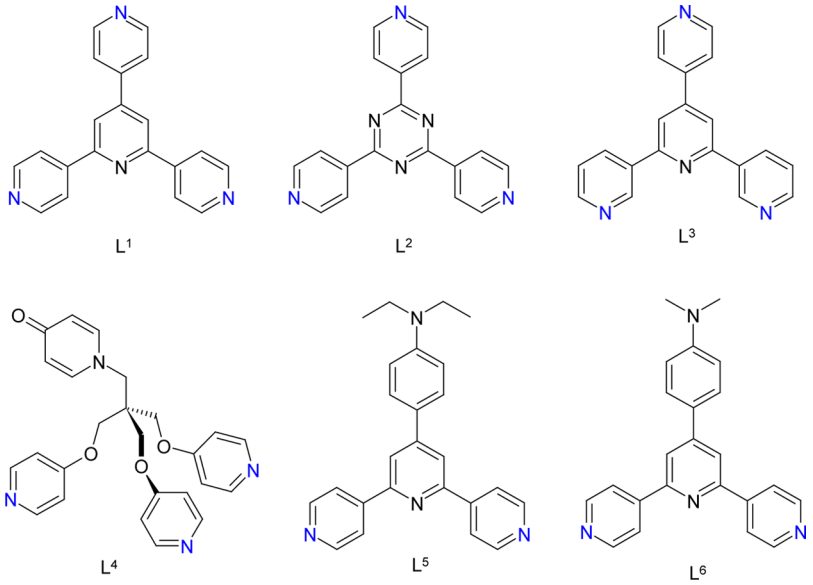

Figure 1. Polypyridine building blocks (nitrogen atoms that coordinate to metal ions are shown in blue).

solvent, stoichiometry, reaction temperature, or time.[6] Polynuclear "building blocks" in the frameworks of PCPs are usually formed by the self-assembly of metal ions and organic ligands in the reaction mixture,[7] or via the decomposition of high nuclearity derivatives.[8] However, the number of examples of presynthesized polynuclear complexes being used as building blocks is much lower.[9−13] Some success in the directed synthesis of PCPs possessing the desired structures can only be expected if a very similar system has already been studied.[14] In particular, the series of similar PCPs was synthesized using the strategy of reticular synthesis.[15] In contrast, the use of polynuclear complexes as building blocks (without undergoing rearrangement during reaction) can lead to the assembly of porous lattices, the structure of which is predetermined to a certain extent by the topology of such blocks and bridging ligands.

In recent years, we reported that the combination of heterometallic trigonal blocks $[Fe_2NiO(Piv)_6]$ (hereinafter abbreviated as $[Fe_2Ni]$) and several polypyridine ligands resulted in coordination polymers or discrete complexes, the topologies of which depend on the symmetry of $[Fe_2Ni]$ blocks and the type of polypyridine spacers.[9−11] The $[Fe_2NiO(Piv)_6]$ can be considered as a pseudotrigonal building block, since both the Fe^{III} and Ni^{II} atoms show the same coordination environments and thus could not be distinguished by the X-ray diffraction analysis. The reaction of $[Fe_2Ni]$ with linear bidentate ligands such as 4,4′-bipyridine (bipy) or *trans*-bis-(4-pyridyl)ethylene (dpe) produced 2D coordination polymers $[Fe_2NiO(Piv)_6(bipy)_{1.5}]_n$ or $[Fe_2NiO(Piv)_6(dpe)_{1.5}]_n$, respectively, which possess honeycomb structures.[10,11] Each honeycomb in a 2D layer of these compounds is constructed from six $[Fe_2Ni]$ moieties linked by six polypyridine ligands, resulting in the interpenetrated layers. The interpenetration is possible due to the sufficiently large size of the cavities in honeycombs. The combination of the same $[Fe_2Ni]$ building block with a pseudotrigonal planar tridentate 2,4,6-tris(4-pyridyl)pyridine ligand (L^1, Figure 1) also gave a 2D coordination polymer $[Fe_2NiO(Piv)_6(L^1)]_n\cdot 3n$DMSO$\cdot 0.84nH_2O$ (**1**) with a honeycomb structure.[9] In contrast to $[Fe_2NiO(Piv)_6(bipy)_{1.5}]_n$ or $[Fe_2NiO(Piv)_6(dpe)_{1.5}]_n$, each honeycomb in $[Fe_2NiO(Piv)_6(L^1)]_n$ is built from three $[Fe_2Ni]$ and three μ_3-L^1 blocks, and the 2D layers are not interpenetrated presumably due to the small cavity size. The linkage of $[Fe_2Ni]$ units by bidentate angular bipyridines resulted in the formation of cyclic structures, namely, a 1D chain with $\{Fe_2NiO(Piv)_6\}_2$(*cis*-dpe)$_2$ cycles in the case of *cis*-bis(4-pyridyl)ethylene (*cis*-dpe), or a discrete 0D "nanocube" $\{Fe_2NiO(Piv)_6\}_8\{L^6\}_{12}$ in the case of bis-2,6-(4-pyridyl)-4-(4-*N*,*N*-dimethylaminophenyl)pyridine (L^6, Figure 1).[9,11] Each of these structures also corresponds to one of the possibly expected topological types.

As a continuation and possible merging of these studies, the present work aimed at investigating the influence of the type of polypyridine ligand on structure and topology of the resulting coordination polymers based on the pseudotrigonal $[Fe_2NiO(Piv)_6]$ blocks. Three analogues of L^1 were used, namely, (i) tris(4-pyridyl)triazine L^2, containing a "central" triazine ring instead of pyridine, (ii) a derivative L^3 that bears two 3-pyridine groups instead of two 4-pyridine rings in L^1 and L^2, and (iii) a tripyridine derivative L^4 that possesses a nonplanar structure in contrast to L^1 and L^2 (Figure 1). As expected, a coordination polymer with L^2, $[Fe_2NiO(Piv)_6(L^2)]_n\cdot 1.25nH_2O$ (**2**), is isostructural to previously reported compound **1**. In contrast, the replacement of L^1 by L^3 or L^4 resulted in the generation of two novel 2D coordination polymers $[Fe_2NiO(Piv)_6(L^3)]_n\cdot 1.5n$DMSO$\cdot 3nH_2O$ (**3**) and $[Fe_2NiO(Piv)_6(L^4)]_n\cdot n$HPiv (**4**), respectively, the topologies of which are different from that of $[Fe_2NiO(Piv)_6(L^1)]_n$ (**1**). In addition, a similar reaction of an analogue of L^6 that comprises a diethylamino group (L^5, Figure 1) was examined, giving rise to a novel double chain 1D polymer $[\{Fe_2NiO(Piv)_6\}_4\{L^5\}_6]_n\cdot 3n$DEF (**5**, where DEF is *N*,*N*-diethylformamide) instead of the discrete 0D "nanocube" $\{Fe_2NiO(Piv)_6\}_8\{L^6\}_{12}\cdot 30$DMF (**6**).

In the present work, we report the synthesis and characterization of **2**, **3**, **4**, and **5**, as well as their structural features and topological analysis. For comparative purposes, the latter has also been performed for **1** and **6**. Since solvent has a significant influence on ordering the crystal lattice of **3** (as evidenced by powder XRD) and its sorption characteristics, two different samples were studied: **3** and **3′** that were synthesized in DMSO or DMF, respectively. For characterization of porous structures

DOI: 10.1021/ic503061z
Inorg. Chem. 2015, 54, 5169−5181

of compounds **2** and **3**, N_2 and H_2 sorption was measured. Sorption of methanol, ethanol, salicylaldehyde, and 9-anthracenecarbaldehyde by **2** was also investigated. Moreover, catalytic activity of **2** in the condensation of aldehydes with malononitrile was evaluated.

EXPERIMENTAL SECTION

General Methods. Commercially available reagents and solvents (Aldrich, Merck) were used as received. The starting materials $[Fe_2NiO(Piv)_6(HPiv)_3]$,[11] tetrakis(*O*-tosyl)pentaerythritol,[16] and 2,4,6-tris-(4-pyridyl)triazine (L^2)[17] were prepared as previously reported. C,H,N-elemental analyses were carried out using a Carlo Erba 1106 analyzer. ^{1}H NMR spectra were recorded on a Varian Unity Plus 400 spectrometer at 400.4 MHz. Chemical shifts are reported in ppm. Powder X-ray diffraction experiments were run on a Bruker D8 instrument with Cu radiation (λ = 1.540 56 Å). UV−vis spectra were measured on a Specord 210 spectrophotometer.

Measurements of N_2 and H_2 sorption were studied on a Sorptomatic-1990 instrument by volumetric method at 78 K, while sorption of methanol and ethanol was investigated gravimetrically at 293 K, as previously described.[12] In order to remove solvent and other compounds that could be captured in the voids, the samples of **2**, **3**, and **3′** were dried in vacuum and hold in acetone for one week (acetone was changed several times) prior to the measurements. The samples were then finally dried in vacuum (10^{-3} Torr) at 150 °C.

Sorption measurements of salicylaldehyde (Sal) or 9-anthracenecarbaldehyde (Aca) by **2** were performed at 373 ± 1 K in hermetic vials as follows: weighed samples of **2** (2×10^{-3} mmol) were mixed with toluene solutions (2 mL) of substrate (c(Sal) was from 0.005 to 0.055 M, c(Aca) = 0.05 M), and the concentration of aldehyde was measured at certain time moments by spectrophotometry at 330 and 405 nm for salicylaldehyde and 9-anthracenecarbaldehyde, respectively. In sorption and catalytic experiments, effective concentration of **2** in suspension was determined as the ratio of a quantity of suspended **2** (in moles) to the volume of solution.

In catalytic experiments, typical reaction mixtures were prepared as follows: aldehyde (0.2 mmol), malononitrile (0.2 mmol), and **2** (2.2×10^{-3} mmol) were continuously stirred in toluene (2 mL) at 100 °C during certain time period (2−40 h). Concentrations of products were measured by ^{1}H NMR.[18] Separate portions of the reaction mixtures were used for determination of conversion versus time. For ^{1}H NMR analysis the following steps occurred: stirring of the reaction mixture was stopped, catalyst was filtered off and washed with hot dichloromethane several times, solvent was evaporated, and the obtained residues were quantitatively dissolved in $CDCl_3$ or DMSO-d_6 for reaction mixtures when using salicylaldehyde or 9-anthracenecarbaldehyde as substrates, respectively. In order to determine conversion of salicylaldehyde, 1,2-dimethoxyethane (0.02 mmol) was added to the probes as standard. Signal with δ = 11.02 ppm was used for integration. In the case of 9-anthracenecarbaldehyde, the standard was not added, and the yields of 2-(9-anthrylmethylene)malononitrile were determined as $\omega = 100\% \times I(\text{product})/[I(\text{product}\} + I(\text{Aca})]$, where I(product) is integral intensity of signal with δ = 9.65 ppm, and I(Aca) is integral intensity of signal with δ = 11.48 ppm. Typical NMR spectra are shown on Figure S1 (Supporting Information).

Control tests for condensations of aldehydes and malononitrile were also performed in the presence of L^2 (2.2×10^{-3} mmol) over 40 h under typical reaction conditions as mentioned above. Concentrations of aldehydes were measured by spectrophotometry. For spectrophotometric measurements, heating and stirring of reaction mixtures was stopped, and aliquots (0.2 mL) of the clear reaction solutions (without particles of L^2) were diluted by toluene (2 mL); spectra of resulting solutions were measured (λ = 320−400 nm in the case of reaction mixtures with Sal, λ = 320−600 nm in the case of reaction mixtures with Aca).

Blank experiments in the absence of any catalyst were also performed by mixing 0.2 mmol of aldehyde with 0.2 mmol of malononitrile in 2 mL of toluene. Reaction mixtures were stirred at 100 °C over 40 h. Concentrations of aldehydes were determined by spectrometry measurements as described above, which confirmed that the condensation reactions do not occur without a catalyst.

Synthesis of L^3. A modified procedure published by Smith et al.[19] was used. 3-Acetylpyridine (10 g, 82.5 mmol) was added to a suspension of crushed NaOH (3.3 g, 82.5 mmol) in polyethyleneglycol PEG-400 (100 mL) and stirred at 0 °C for 10 min. 4-Pyridinecarboxaldehyde (4.42 g, 41.2 mmol) was then added, and the suspension was left standing at 0 °C for 2 h. Every 30 min the mixture was manually stirred with a spatula. After 2 h, NH_4OAc (20 g, excess) was added, and the suspension was heated at 110 °C for 10 h. During this time, the color of the mixture changed from cherry-red to auburn, and a precipitate of the product formed. Water (200 mL) was then added, and the precipitate was isolated by filtration and washed with water (100 mL) and cold acetone (20 mL). Recrystallization from $CHCl_3$ gave white solid, yield 9 g (70%). Anal. Found/Calcd for $C_{20}H_{14}N_4$, %: C, 77.3/77.4; H, 4.55/4.55; N, 18.2/18.1.

Synthesis of L^4. 4-Hydroxypyridine (0.95 g, 10 mmol), tetrakis(*O*-tosyl)pentaerythritol (1.88 g, 2.5 mmol), and K_2CO_3 (5 g) were heated under reflux in DMSO (50 mL) for 8 h. Then, the reaction mixture was cooled down to room temperature and poured in 250 mL of water. The obtained precipitate was filtered off, recrystallized from chloroform, and dried in vacuum over P_2O_5. Yield 0.10 g (10%). Anal. Found/Calcd for $C_{25}H_{24}N_4O_4$, %: C, 67.8/67.6; H, 5.55/5.44; N, 12.5/12.6.

Synthesis of L^5. The synthetic procedure was similar to that for L^3, with the difference that 4-acetylpyridine (10 g, 82.5 mmol) was used instead of 3-acetylpyridine, and *p*-diethylaminobenzaldehyde (7.3 g, 41.2 mmol) was applied instead of 4-pyridinecarboxaldehyde. For the isolation of the product, water (150 mL) was added, and the precipitate was removed by filtration and washed with H_2O (100 mL) and cold acetone (40 mL). Recrystallization from acetone gave yellow solid, yield 7.0 g (45%). Anal. Found/Calcd for $C_{24}H_{24}N_4$, %: C, 78.3/78.2; H, 6.55/6.57; N, 15.3/15.2.

Synthesis of Compound 2. A solution of $[Fe_2NiO(Piv)_6(HPiv)_3]$ (0.198 g, 0.18 mmol) in DMF (15 mL) was slowly added to a DMF solution (60 mL) containing L^2 (0.066 g, 0.21 mmol) and pivalic acid (0.81 g, 7.93 mmol), and the reaction mixture was heated at 120 °C for 1 h resulting in the formation of yellowish-green microcrystals. These were collected by filtration, held in acetone for 3 days, and then filtered off and dried in vacuum. Yield 0.190 g (95%). Anal. Found/Calcd for $Fe_2NiC_{48}H_{68.5}N_6O_{14.25}$, $[Fe_2NiO(Piv)_6(L^2)]_n \cdot 1.25nH_2O$, %: C, 50.9/51.1; H, 5.92/6.12; N, 7.46/7.45. Water molecules were captured from air prior to elemental analysis.

Synthesis of Compound 3. Synthesis was carried out using the same procedure as for **2**, with the difference that L^3 (0.065 g, 0.21 mmol) was used instead of L^2. Two alternative solvents were used: DMSO or DMF. Yield of **3** in the reaction with DMSO as solvent was 0.22 g (95%). Anal. Found/Calcd for $C_{53}H_{83}N_4O_{17.5}S_{1.5}Fe_2Ni$, $[Fe_2NiO(Piv)_6(L^3)]_n \cdot 1.5n\text{DMSO} \cdot 3nH_2O$, %: C 49.9/49.9; H 6.21/6.56; N 4.58/4.40. Water molecules were captured from air prior to elemental analysis. Yield of **3′** in the reaction with DMF as solvent was 0.190 g (95%). Anal. Found/Calcd for $C_{50}H_{70}N_4O_{14}Fe_2Ni$, $[Fe_2NiO(Piv)_6(L^3)]_n \cdot nH_2O$, %: C, 53.2/53.6; H, 5.99/6.29; N, 4.89/5.00. Water molecule was captured from air prior to elemental analysis.

Synthesis of Compound 4. A solution of L^4 (0.022 g, 0.05 mmol) in DMF (10 mL) was added to a DMF/MeCN (40 mL/20 mL) solution containing $[Fe_2NiO(Piv)_6(HPiv)_3]$ (0.055 g, 0.05 mmol) and HPiv (0.05 g, 0.49 mmol). Greenish-brown crystals formed in 3 days and were then collected and dried in air. Yield 0.03 g (50%). Anal. Found/Calcd for $C_{60}H_{88}N_4O_{19}Fe_2Ni$, $[Fe_2NiO(Piv)_6(L^4)]_n \cdot n\text{HPiv}$, %: C, 53.6/53.8; H, 6.80/6.62; N, 4.10/4.18.

Synthesis of Compound 5. A solution of $[Fe_2NiO(Piv)_6(HPiv)_3]$ (0.030 g, 0.027 mmol) in acetonitrile (6 mL) was carefully layered over an *N*,*N*-diethylformamide (DEF) solution (2 mL) containing L^5 (0.019 g, 0.05 mmol) and HPiv (0.06 g, 0.58 mmol). Dark greenish-brown crystals were formed in 10 days and then were collected and dried in air. Yield 0.03 g (50%). Anal. Found/Calcd for $C_{279}H_{393}N_{27}O_{55}Fe_8Ni_4$, $[\{Fe_2NiO(Piv)_6\}_4(L^2)_6]_n \cdot 3n\text{DEF}$, %: C, 59.2/58.9; H, 7.00/6.97; N, 6.45/6.65.

DOI: 10.1021/ic503061z
Inorg. Chem. 2015, 54, 5169−5181

Table 1. Crystal Data and Structure Refinement Details for 2−5

	2	3	3
empirical formula	$C_{48}H_{66}Fe_2N_6NiO_{13}$	$C_{50}H_{68}Fe_2N_4NiO_{13}$	$C_{50}H_{68}Fe_2N_4NiO_{13}$
fw (g mol^{-1})	1105.48	1103.49	1103.49
temp (K)	150(2)	160(2)	230(2)
wavelength (Å)	0.710 73	0.710 73	0.710 73
cryst size, mm^3	0.15 × 0.1 × 0.1	0.2 × 0.1 × 0.1	0.1 × 0.1 × 0.1
cryst syst	trigonal	monoclinic	monoclinic
Space group	$P\bar{3}_1/c$	$P2_1/c$	$P2_1/c$
a (Å)	16.667(5)	13.1615(11)	13.164(4)
b (Å)	16.667(5)	16.9299(14)	17.071(5)
c (Å)	14.966(4)	30.922(3)	31.150(9)
β (deg)	90	92.319(2)	92.110(6)
V (Å^3)	3600(2)	6884.5(10)	6996(4)
Z	2	4	4
calcd density (g cm^{-3})	1.020	1.065	1.048
abs coeff (mm^{-1})	0.705	0.736	0.724
F(000)	1160	2320	2320
θ range for data collection (deg)	1.41−23.31	1.32−25.69	1.31−25.69
refns collected	19 891	58 968	57 839
reflns unique	1751	13 092	13 291
R(int)	0.1502	0.1362	0.2014
params	121	631	631
GOF on F^2	1.206	0.834	0.817
R1 ($[I > 2\sigma(I)]$[a]	0.0752	0.0622	0.0774
wR2 $[I > 2\sigma(I)]$[b]	0.2301	0.1419	0.1805

	4	5
empirical formula	$C_{60}H_{87}Fe_2N_4NiO_{19}$	$C_{135}H_{180}Fe_4N_{12}Ni_2O_{26}$
fw (g mol^{-1})	1338.75	2727.73
temp (K)	296(2)	296(2)
wavelength (Å)	0.71073	0.71073
cryst size, mm^3	0.12 × 0.08 × 0.01	0.20 × 0.15 × 0.1
cryst syst	monoclinic	monoclinic
space group	$P2_1/n$	$P2_1$
a (Å)	11.917(6)	12.514(2)
b (Å)	34.750(18)	60.998(9)
c (Å)	23.067(12)	12.873(2)
β (deg)	98.817(8)	98.645(3)
V (Å^3)	9439(9)	9714(3)
Z	4	2
calcd density (g cm^{-3})	0.942	0.933
abs coeff (mm^{-1})	0.550	0.532
F(000)	2828	2884
θ range for data collection (deg)	1.07−26.41	0.67−25.69
reflns collected	75 894	42 413
reflns unique	19 292	29 160
R(int)	0.1734	0.1245
params	765	1237
GOF on F^2	0.722	0.841
R1 ($[I > 2\sigma(I)]$[a]	0.0763	0.1013
wR2 $[I > 2\sigma(I)]$[b]	0.1798	0.2270

[a] $R1 = \sum||F_o| - |F_c||/\sum|F_o|$. [b] $wR2 = \{\sum[w(F_o^2 - F_c^2)^2]/\sum[w(F_o^2)^2]\}^{1/2}$.

X-ray Crystal Structure Determinations. The X-ray data sets for the compounds **2**, **3**, **4**, and **5** were collected on a Bruker APEX II diffractometer equipped with a CCD camera and a graphite monochromated Mo Kα radiation source (λ = 0.710 73 Å).[20] The X-ray quality crystals of compounds **4** and **5** were taken from the reaction mixtures, while single crystals of **3** were grown by diffusion of diethyl ether into solution of starting compound in DMSO. In the case of **2**, X-ray data were collected using an air-dried sample in order to check the stability of the crystal structure upon desolvation (isostructural nature of **1** and **2** was confirmed by single-crystal unit cell measurements and powder XRD). X-ray data for **3** were collected at 160 and 230 K. The structures were solved using SHELXS-97[21] and refined with SHELXL-97[21] by full-matrix least-squares on F^2. The H atoms were treated by a riding model. Disordered solvent molecules in compounds **3** (at 230 K), **4**, and **5** could not be localized, and thus, the corresponding electronic density was corrected by SQUEEZE.[22] Table 1 contains crystal data. CCDC deposition numbers are 1040164−1040168 for **2**, **3** (160 K), **3** (230 K), **4**, and **5**, respectively. The channel diameters in **1**, **2**, and **3** were estimated from the Mercury diagram for a probe molecule with r = 1.4 Å, taking into account that

DOI: 10.1021/ic503061z
Inorg. Chem. 2015, 54, 5169−5181

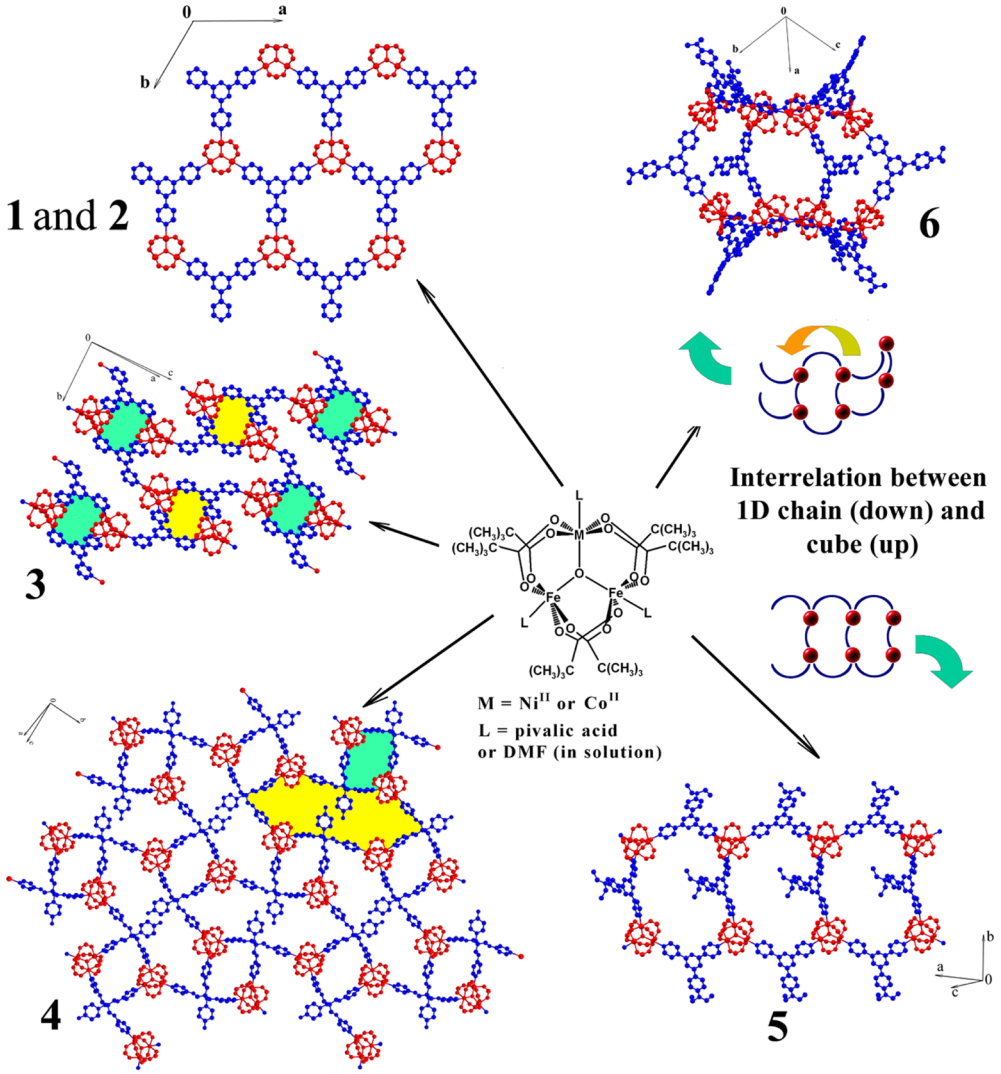

Figure 2. Scheme illustrating the formation of **1**–**6** and their structural fragments. All H atoms, *t*-Bu groups, and noncoordinated molecules (if any) are omitted for clarity. In **3**, planes marked by yellow or green belong to sets; planes within each set are parallel, but planes from different sets are inclined *ca.* 85° to each other. In **4**, yellow and green indicate different metallocycles. Structural fragments of **1** and **6** are drawn using published data.[9]

the image of the channel corresponds to the centers of spheres that touch channel "wall", and a true channel is 2*r* wider.

RESULTS AND DISCUSSION

Synthesis. Synthesis of the L^3 and L^5 ligands was performed similarly to reported procedures.[19] The preparation of L^4 involved a reaction of tetrakis(*O*-tosyl)pentaerythritol with 4-hydroxypyridine, similar to reported procedures.[23] However, instead of the expected derivative with four 4-pyridine groups, a different compound was obtained that bears one N-substituted 4-pyridone fragment (Scheme S2, Supporting Information). This group formed as a result of N-alkylation of 4-hydroxypyridine instead of O-alkylation.

The coordination polymers $([Fe_2NiO(Piv)_6(L^2)]_n \cdot 1.25nH_2O)$ **2**, $([Fe_2NiO(Piv)_6(L^3)]_n \cdot 1.5n\text{DMSO} \cdot 3nH_2O)$ **3**, $([Fe_2NiO(Piv)_6(L^4)]_n \cdot n\text{HPiv})$ **4**, and $([\{Fe_2NiO(Piv)_6\}_4\{L^5\}_6]_n \cdot 3n\text{DEF})$ **5** were synthesized via treatment of $[Fe_2NiO(Piv)_6(HPiv)_3]$ with the corresponding polypyridine spacers, with adoption of the protocols reported for related compounds.[9−11] In all cases the total number of donor atoms in polypyridine ligands that can be bound by the metal ions in the $[Fe_2Ni]$ unit (i.e., N atoms of central pyridine and dialkyamino groups, and all O atoms of L^4 were not counted) was equal to a number of "free" coordination sites in $[Fe_2NiO(Piv)_6]$, thus allowing a comparison of the observed and expected structures.

Two samples were prepared by the reaction of $[Fe_2NiO(Piv)_6(HPiv)_3]$ with L^2 in DMSO or DMF (**3** and **3′**, respectively), which possess the same ratio of $[Fe_2Ni]$ trinuclear block and L^2, but differ by solvent composition. Despite being rather similar, these samples exhibit significantly distinct sorption properties, which can be explained by different crystallinity of these compounds, *vide infra*.

Crystal Structures. *Compound 2.* Compound **2** is isostructural to a previously characterized derivative **1**,[9] as confirmed by powder X-ray data (see Figure S3, Supporting Information) and unit cell parameters measured for a single crystal. In order to check the stability of crystal lattice of **2** upon desolvation, the X-ray data were collected using a crystal dried in air for several days. It was found that a single crystal of **2** preserves crystallinity under these conditions, and the crystal structure was successfully solved. Unit cell parameters *a* and *b* for **2** were 0.1 Å lower compared to those of **1** (16.667(5) Å in

DOI: 10.1021/ic503061z
Inorg. Chem. 2015, 54, 5169−5181

2 vs 16.775(2) Å in **1** at the same temperature), while the values of *c* were closer (14.966(4) Å vs 14.973(2) Å, respectively). We suppose that these differences are not caused by solvent content in voids, but by the replacement of a central pyridine ring in **1** into a triazine one in **2**. Since the L^1 and L^2 structures have a local C_3 axis, the C−C and C−N bonds in central rings were averaged in the structural model. These average values were equal to 1.341(6) Å in **2** and 1.364(6) Å in **1**, and can be responsible for unit cell contraction, even despite slightly longer M−N bonds in **2** compared to **1** (2.192(7) vs 2.175(7) Å, respectively). Other structural features, including porosity characteristics, are almost the same for **1** and **2**. Crystal lattice of **2** features similar channels with the cavity diameter of ∼10.6 Å, window diameter of ∼6.4 Å, and pore volume of ∼0.24 cm^3/g (estimated from X-ray data by Platon[24] for a probe molecule with r = 1.4 Å).[25]

Compound ***3***. The crystal structure of **3** was solved using the data collected at two temperatures, 160 and 230 K. Though main features of the structure at these temperatures are similar, only low-temperature modification will be described in detail and significant differences will be noted.

The crystal structure of **3** features the corrugated 2D layers (Figure 2 and Supporting Information Figures S6, S7). Similarly to **1** and **2**, each L^3 moiety is bound to three $[Fe_2Ni]$ units. The L^3 spacers are almost planar (the largest deviation of carbon atoms from the mean plane of L^3 is 0.217(2) Å at 160 K or 0.209 Å at 230 K), which is essential for the formation of a network with a predetermined topology (Figure 3). Two adjacent $[Fe_2Ni]$ blocks are linked by two L^3 ligands in such way that the centrosymmetric cyclic $[Fe_2Ni]_2(L^3)_2$ motifs can be distinguished (highlighted by yellow and green in Figure 2 and separately shown in Figure 3). Each $[Fe_2Ni]_2(L^3)_2$ motif has a structure resulting from the combination of a trigonal metal-containing building block and rigid ligand, which predetermine the 60° angle between the M−N bonds (where M are metal atoms of different trinuclear blocks, Figure 3). The metal atoms in each $[Fe_2Ni]_2(L^3)_2$ cyclic motif lie in one plane, and the angle between the mean planes of the adjacent motifs (yellow and green in Figure 2) is 84.14° at 160 K (83.20° at 230 K). Four above-mentioned $[Fe_2Ni]_2(L^3)_2$ cyclic fragments form a larger ring-containing void (*vide infra*).

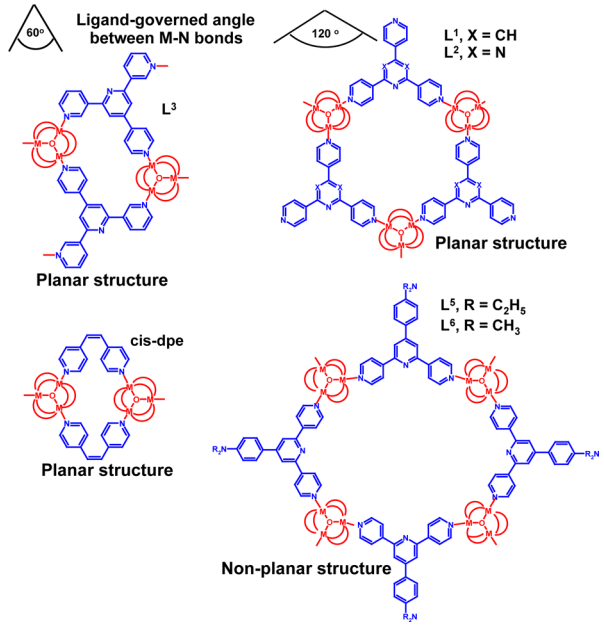

Figure 3. Metallocycles $[Fe_2Ni]_x(L)_y$ formed as a result of junction of trinuclear pivalate with various polypyridines in different combinations in **1**−**3**, **5**, **6**, and related compound derived from *cis*-(4-pyridyl)-ethylene (*cis*-dpe).[11]

Due to the fact that the arrangement of 2D layers in **3** can be considered as a result of translation along the *a* axis without a shift, the voids of each 2D layer are arranged in channels along the *a* axis (Figure 4). Such channels can be presented as a consequence of cavities (diameter ∼13.8 Å) separated by windows (diameter ∼8.1 Å). Solvent-accessible volume of voids in **3**, estimated by PLATON, is equal to 27% at 160 K (28% at 230 K) for a probe molecule with r = 1.4 Å, corresponding to the pore volume of ∼0.25 cm^3/g. As can be seen from structural data, the channels in **3** are bigger than those in **1** because they are located inside a larger $\{[Fe_2Ni]_2(L^3)_2\}_4$ "cycle" compared to $[Fe_2Ni]_3(L^1)_3$ in **1**. However, the total solvent-accessible volumes in **1** and **3** are close, which is consistent with more "thick" walls between the channels in **3**.

Compound ***4***. The crystal lattice of the coordination polymer **4** is built from 2D layers (Figure 2). Each L^4 spacer acts as a tridentate ligand and links three $[Fe_2Ni]$ units, while each $[Fe_2Ni]$ block is bound by three L^4 moieties (Figure S4, Supporting Information). Every L^4 ligand participates in the formation of two different metallocycles, which involve two and four $[Fe_2Ni]$ units, respectively (marked by green and yellow in Figure 2). All metal ions within the metallocycle containing two $[Fe_2Ni]$ units lie in one plane, while the neighboring metallocycles of this type are not coplanar. Thus, the bent character of 2D layers is consistent with a nonplanar structure of L^4, in contrast to L^1 and its perfectly planar derivative **1**.[9] The adjacent 2D layers are shifted with a distance of 5.244 Å, which is estimated as the separation between the parallel mean planes that go through metal ions in the $[Fe_2Ni]$ units from the adjacent layers. The pyridone rings of L^4 from the neighboring layers are coplanar and located at 3.396 Å from each other (the distance between the mean planes of such rings, Supporting Information Figure S5), indicating some stacking interactions between them.

Compounds ***5*** *and* ***6***. The compound **5** is a 1D coordination polymer with a double chain structure, wherein two $\{[Fe_2Ni](L^5)\}_n$ chain motifs are held together via additional linkage of L^5 between each $[Fe_2Ni]$ unit (Figure 2). Alternatively, **5** can be considered as a series of 24-membered units $[Fe_2Ni]_4(L^5)_4$ interconnected by the L^5 linkers. As expected,[9] the $[Fe_2Ni]_4(L^5)_4$ fragments are not planar. Previously, we reported a related compound $[Fe_2Ni]_8(L^4)_{12}$ (**6**) with a cube-like structure.[9] The replacement of dimethylamino group in L^6 by a diethylamino moiety in L^5 led to the formation of a 1D chain structure in **5** instead of "folding" into a 0D cube (Figure 2). Cube-like molecules of **6** were polycatenated in the solid state.[9] It can be assumed that such polycatenation was important to stabilize the crystal lattice and decrease ΔG of compound **6** formation. In such a case, a possible reason for the difference between the topologies of **5** and **6** can consist of a larger size of the diethylamino group over the dimethylamino group in L^5 and L^6, respectively. In **6**, there is a short contact between the H atoms of dimethylamino group of L^6 of one cube and the H atoms of *tert*-butyl group of $[Fe_2NiO(Piv)_6]$ of adjacent cube (Figure S8, Supporting Information). Hence, there is probably no enough space for

DOI: 10.1021/ic503061z
Inorg. Chem. 2015, 54, 5169−5181

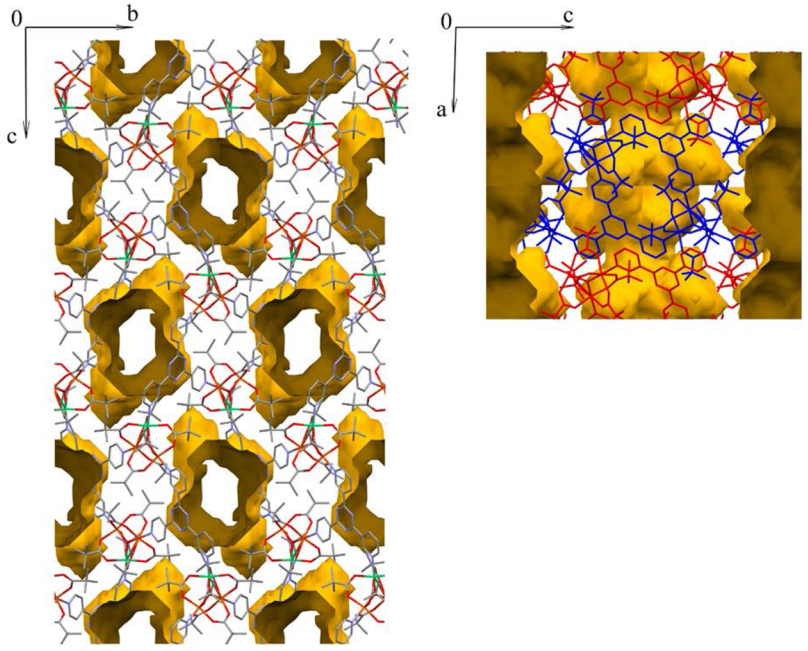

Figure 4. Visualization of voids in the crystal structure of **3** (160 K). Mercury diagram drawn for a probe molecule with r = 1.4 Å. Projections along the a and b axes.

the ethyl group in a hypothetic polycatenated cubic structure, which leads to the formation of a chain. The adjacent 2D layers in **5** are arranged in such a way that no apparent voids are formed (Supporting Information Figure S9).

Topological Diversity of 1–6. To get further insight into the structures of 2D (**1**–**4**), 1D (**5**), and 0D (**6**) networks, we have performed their topological analysis.[26] Following the concept of the underlying net,[27,28] all the μ-Piv and μ-L^{1-6} moieties in **1**–**6** have been reduced to their centroids resulting in simplified metal–organic networks.

Thus, an underlying net of **2** is composed of the 4-connected Fe and Ni nodes (topologically equivalent), 3-connected μ_3-L^2 and μ_3-O nodes, as well as 2-connected μ_2-Piv linkers (Figure 5a and Figure S10, Supporting Information). This trinodal 3,3,4-connected net possesses a rare 3,3,4L40 topology[26,29] expressed by the point symbol of $(3^3.9^2.10)_3(3^3)(9^3)$, with the $(3^3.9^2.10)$, (3^3), and (9^3) indices corresponding to the Fe/Ni, μ_3-O, and μ_3-L^2 nodes, respectively. This network can be reduced further to a uninodal 3-connected net with the hcb [Shubnikov hexagonal plane net (6,3)] topology and the point symbol of (6^3) (Figure 5a), after treating the heterometallic $[Fe_2Ni(\mu_3\text{-O})(\mu\text{-Piv})_6]$ blocks as the 3-connected cluster nodes. The compound **1** is topologically similar to **2**.

From the topological viewpoint, the underlying 2D networks of **3** and **4** are similar. These are assembled from the 4-connected Fe and Ni nodes, 3-connected μ_3-O and μ_3-$L^{3,4}$ nodes, and 2-connected μ-Piv linkers (for **3**, see Figure 5b and Supporting Information Figure S10). Their topological analysis[26] discloses the complex tetranodal 3,3,4,4-connected networks with a unique topology described by the point symbol of $(3^3.12^2.13)(3^3.6.7^2)_2(3^3)(6.12^2)$, wherein the $(3^3.12^2.13)$, $(3^3.6.7^2)$, (3^3), and (6.12^2) notations correspond to the Ni, Fe, μ_3-O, and μ_3-$L^{3,4}$ nodes, respectively. Further simplification of the obtained networks, namely, by considering the heterometallic $[Fe_2Ni(\mu_3\text{-O})(\mu\text{-Piv})_6]$ blocks as the 3-connected cluster nodes, furnishes the uninodal 3-connected nets (for **3**, see Figure 5b) with the fes [Shubnikov plane net] topology and the point symbol of (4.8^2).[26,30,31] Although various compounds with the fes topology have been described,[32] **3** and **4** reveal the first example of the present topological type that is assembled

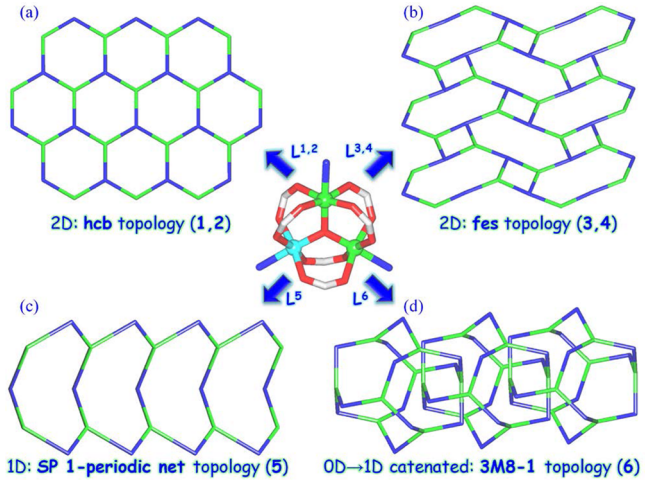

Figure 5. Topological representations of the simplified uninodal 3-connected networks in **2** (a), **3** (b), **5** (c), and **6** (d) after contracting the $[Fe_2Ni(\mu_3\text{-O})(\mu\text{-Piv})_6]$ units to 3-connected cluster nodes (second simplification; for initial simplification, see Supporting Information Figure S10). (a) 2D net with the hcb [Shubnikov hexagonal plane net (6,3)] topology and the point symbol of (6^3) (view along the c axis). (b) 2D net with the fes [Shubnikov plane net] topology and the point symbol of (4.8^2). (c) 1D chain with the SP 1-periodic net (4,4)(0,2) topology and the point symbol of $(4^2.6)$. (d) 0D → 1D catenated net with the 3M8-1 topology and the point symbol of (4^3). Networks shown in parts b, c, and d are along the a axis. Further details: $[Fe_2Ni(\mu_3\text{-O})(\mu\text{-Piv})_6]$ cluster node is shown in the center [t-Bu groups of μ-Piv are omitted for clarity; Fe (green), Ni (cyan), O (red), C (gray)]; (a–d) centroids of $[Fe_2Ni(\mu_3\text{-O})(\mu\text{-Piv})_6]$ cluster nodes after simplification (green), centroids of μ_3-$L^{1,3}$ nodes or μ_2-$L^{5,6}$ linkers (blue).

DOI: 10.1021/ic503061z
Inorg. Chem. 2015, 54, 5169–5181

from a μ_3-oxo trimetallic hexacarboxylate cluster $[M_3(\mu_3\text{-}O)(\mu\text{-}RCOO)_6]$ as a secondary building unit (SBU).[26,30,33]

After simplification procedure, the obtained trinodal 3,3,4-connected double chain of **5** (Figure 5d and Supporting Information Figure S10) can be topologically described by the point symbol of $(3^3.8.9^2)_2(3^3.8^2.9)(3^3)$ with the $(3^3.8.9^2)$, $(3^3.8^2.9)$, and (3^3) notations corresponding to the 4-connected Fe1/Fe3/Ni1/Ni2, 4-connected Fe2/Fe4, and 3-connected μ_3-O nodes, respectively. Further simplification of this topologically unique 1D network by treating the $[Fe_2Ni(\mu_3\text{-}O)(\mu\text{-}Piv)_6]$ units as 3-connected cluster nodes and μ_2-L^5 moieties as 2-connected linkers furnishes a uninodal net (Figure 5d) with a rare SP 1-periodic net (4,4)(0,2) topology[26] defined by the point symbol of $(4^2.6)$.

The underlying structure of **6** is composed of the discrete 0D clusters that are catenated into a 1D array. The topological analysis reveals a binodal 3,4-connected net (Figure 5c and Supporting Information Figure S10) that features an unreported topology[26,28,30,33] described by the point symbol of $(3^3.8^2.9)_3(3^3)$, wherein the $(3^3.8^2.9)$ and (3^3) indices are those of the 4-connected Fe and Ni nodes (topologically equivalent) and 3-connected μ_3-O nodes, respectively. The $[Fe_2Ni(\mu_3\text{-}O)(\mu\text{-}Piv)_6]$ blocks can be contracted to the 3-connected cluster nodes which, along with the 2-connected μ_2-L^6 linkers, give rise to a further simplified uninodal net (Figure 5c) with the 3M8-1 topology and the point symbol of (4^3). The present type of topology is very rare and has been reported only in a single case.[34]

*Thermal Stability and Sorption Properties of **2**, **3**, and **3′**.* Partial or complete desolvation of **2** has almost no influence on its crystal structure, as confirmed by comparison of powder XRD patterns (Supporting Information Figure S11) and successful X-ray structure determination of the desolvated crystal. Only some redistribution of relative intensities of reflections was observed in the experimental patterns compared to calculated ones. All expected reflections were found on experimental patterns.

In contrast, the powder XRD pattern of air-dried sample of **3**, prepared in DMSO (the same solvent as used for single-crystal growth), contains wide reflections which are evidence for poor crystallinity of the bulk sample of this compound or small particle size (Supporting Information Figure S12). While positions of these reflections correspond to the expected ones (with some redistribution of relative intensities, as in the case of **2**), some expected reflections are not found. In particular, all low-angle reflections (at 2θ = 5.6°, 5.9°, and 6.7°, which correspond to 002, 011, and 100 planes, respectively) are absent, and there is also no reflection at 2θ = 18.7 ° (12−5 plane). Reflections expected between 2θ = 8.5° and 9.0° (planes 110, 003, 10−2, 11−1, 102, and 111) merge in the experimental powder XRD pattern of **3**.

As mentioned in the Experimental Section, the reaction between the same reagents in DMF instead of DMSO led to the formation of sample **3′**. Surprisingly, powder XRD pattern of **3′** contained more distinct and narrow reflections, which fit much better to the expected powder XRD pattern (Supporting Information Figure S12). The dominating majority of expected reflections was found (redistribution of relative intensities occurred).

Heating of samples **2** and **3′** in 10^{-3} Torr vacuum, performed for activation prior to sorption measurements, did not lead to significant structural changes, as evidenced by comparison of their powder XRD patterns with X-ray diffraction for nonactivated samples (Supporting Information Figures S11 and S12). Under the same conditions, the crystallinity of **3** slightly deteriorated, and reflections on the PXRD pattern became wider and less intense.

Since crystallographic studies showed that only compounds **2** and **3** possess voids in crystal lattices, sorption properties of **4** and **5** were not studied (sorption properties of **1** and **6** were previously reported [9]). Bearing in mind a significant difference between powder XRD patterns for **3** and **3′** ($[Fe_2NiO(Piv)_6L^3]_n$, sorption properties of both samples were investigated.

Desolvated compounds **2**, **3**, and **3′** exhibit permanent porosity, which has been confirmed by sorption of N_2 and H_2 at 78 K (Figure 6a,b). Nitrogen adsorption isotherms for compounds **2** and **3′** are typical for microporous sorbents.[35] A sharp growth of N_2 adsorption up to 150 and 40 $cm^3\ g^{-1}$ at a

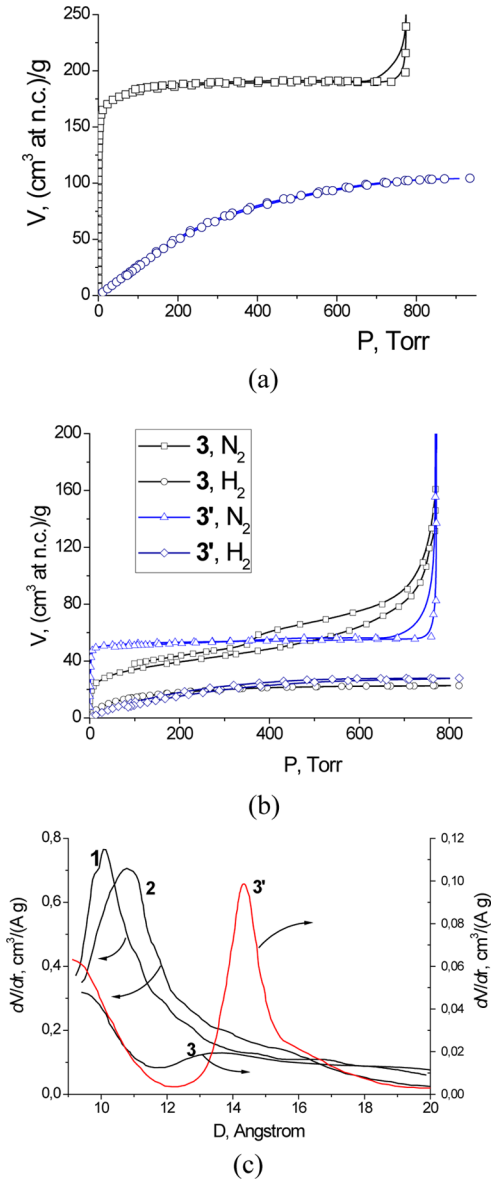

Figure 6. (a) Isotherms of N_2 (□) and H_2 (○) sorption for **2**; (b) isotherms of N_2 (□) and H_2 (○) sorption for **3**, and N_2 (△) and H_2 (◇) sorption for **3′**; (c) Saito−Foley distribution of micropores with diameter (D) derived from N_2 adsorption data for **1**−**3**. dV/dr for **1** was calculated on the basis of published data.[9]

DOI: 10.1021/ic503061z
Inorg. Chem. 2015, 54, 5169−5181

very low pressure (3 Torr) for **2** and **3′**, respectively, is caused by micropores filling. The second sharp growth of N_2 adsorption isotherms at P close to P_S can be explained by interparticle condensation. The N_2 sorption is completely reversible for both these compounds. At the same time, the shape of nitrogen sorption isotherm of **3** indicates the presence of not only regular micropores, but also a significant contribution of irregular mesopores. Adsorption isotherm for **3** continuously grows after micropores filling at PP_S^{-1} between 3 and 750 Torr (Figure 6b). In addition, there is a small hysteresis of N_2 adsorption−desorption in **3**, which is absent in **2** and **3′**. The difference between the N_2 sorption for compounds **2** and **3′** on one side versus **3** on the another side is consistent with their powder XRD patterns (*vide supra*). In fact, compounds **2** and **3′** possess high crystallinity, while **3** is significantly disordered.

For **2**, the micropore volume estimated using the Dubinin−Radushkevich approach (V_{DR} = 0.29 cm^3 g^{-1}, Table 2) is consistent with the value calculated from crystallographic data (0.24 cm^3 g^{-1}). In contrast, V_{DR} is significantly lower for both **3** and **3′** (0.03 and 0.08 cm^3 g^{-1}, respectively, Table 2) than the value expected from the X-ray structure (0.25 cm^3 g^{-1}). This difference can be explained by partial blocking of micropores or crystal structure disorder (more significant for **3**, less significant for **3′**). Sorption properties of **2** resemble those of its isostructural analogue **1** (Table 2).[9]

Table 2. Parameters of N_2 and H_2 Sorption Isotherms of 1−3

compd[a]	S_{BET}, m^2 g^{-1}[b]	V_{DR}, cm^3 g^{-1}	$u(H_2)$, % by weight	ref
1	730	0.28	0.91	9
2	730	0.29	0.93	this work
3	140	0.03	0.20	this work
3′	205	0.08	0.25	this work

[a]All compounds were desolvated in vacuum prior to sorption measurements. [b]S_{BET}, V_{DR}, and $u(H_2)$ stand for BET surface area, Dubinin−Radushkevich micropore volume, and the highest experimentally achieved hydrogen capacity at 78 K, respectively.

The diameter of micropores (D) was estimated from N_2 adsorption isotherms by the Saito−Foley model using potential function derived for N_2 on zeolite at 77.3 K as an approximation.[36] Such an approach gave the D values of ∼10.0 and ∼10.8 Å (maxima of dV/dr curves, Figure 6c) for **1** and **2**, respectively. These values are consistent with crystallographic data (*vide supra*). A similar analysis performed for **3** and **3′** showed maxima of dV/dr at D of ∼13.6 and ∼14.3 Å, respectively, which fit well with the value expected from the X-ray structure of **3**. Notably, the dV/dr curve for **3** has a second poorly defined maximum at D ∼18.9 Å, which can be considered as a numerical estimation of effective average diameter of "additional" irregular pores present in the sample. Surprisingly, hydrogen sorption capacity values for **3** and **3′** are very close (Figure 6b and Table 2). This can be rationalized assuming that channels in the crystal lattice of **3** are partially blocked and not accessible for N_2 (r = 3.64 Å),[37] but are accessible to H_2 (r = 2.8 Å). Notably, close values of H_2 sorption for **3** and **3′** can be considered as an argument, confirming that (i) there is no impurity of nonporous phase in these samples, and (ii) possible presence of such impurity cannot be responsible for the difference between N_2 sorption isotherms for these compounds.

To get additional information about accessibility of pores of **2** to various substrates, sorption of methanol and ethanol was measured at 293 K from the gaseous phase, and sorption of salicylaldehyde and 9-anthracenecarbaldehyde was studied from toluene solution at 373 K as well. Both isotherms of alcohol sorption reach saturation at V of ∼0.3 cm^3 g^{-1} (Figure 7) that is very close to V_{DR} calculated from N_2 adsorption (Table 2), providing evidence that **2** possesses "rigid" micropores, which do not change on interaction with guest molecules in contrast to previously reported cases.[11,12,38,39] This observation is consistent with powder XRD data, which indicate that the crystal lattice of **2** is stable upon desolvation (*vide supra*). Pressure decrease to zero leads to complete desorption of methanol without significant hysteresis, providing evidence that MeOH is not bound by covalent bonds. In fact, coordination to metal ion is impossible, because there are no free sites available in **2**.

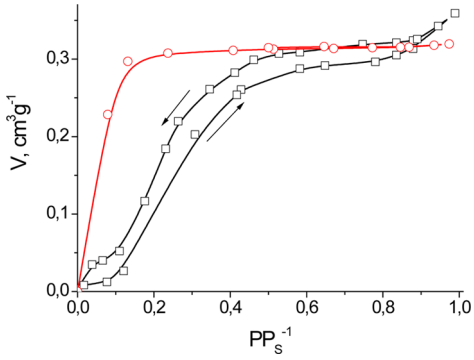

Figure 7. Isotherms of methanol (□) and ethanol (○) sorption by **2** at 293 K. Arrows indicate direction of isotherm at absorption and desorption.

Isotherm of ethanol absorption reaches saturation at lower PP_S^{-1}, compared to methanol absorption (Figure 7). This can be explained by a higher affinity of more hydrophobic ethanol (compared to methanol) to hydrophobic *tert*-butyl groups of $[Fe_2NiO(Piv)_6]$ units. These results are consistent with the difference, observed previously between methanol and ethanol absorption by pivalate-based coordination polymers $[Fe_2MO(Piv)_6(L)_{1.5}]_n$ (M = Co^{II} or Ni^{II}, L = 4,4′-bipyridine or *trans*-1,2-bis(4-pyridyl)ethylene).[11,12] Though the absorption of alcohol by $[Fe_2MO(Piv)_6(L)_{1.5}]_n$ probably led to expansion of the crystal lattice due to rearrangement of 2D layers (and alcohol absorption could not be considered as filling of rigid micropores), ethanol sorption capacity was higher than that of methanol.[11,12]

Catalytic Activity of 2 in Aldehyde Condensation with Malononitrile. Compound **2** can be considered as a potential heterogeneous catalyst for condensation reactions that can be catalyzed by N atoms of triazine rings in pores, similarly to reported cases.[40−42] Hence, condensation of salicylaldehyde or 9-anthracenecarbaldehyde with malononitrile was studied in the present work. For analysis of catalytic results (*vide infra*), sorption of salicylaldehyde from toluene solution at T = 373 K was investigated. In contrast to sorption of N_2 or H_2, isotherm of salicylaldehyde sorption by **2** was not typical for pores filling in microporous sorbent (Figure 8a). Noticeable sorption begins at equilibrium salicylaldehyde concentration c(Sal) ≈ 7 × 10^{-3} M, and then the adsorption isotherm continuously rises, reaching the sorption capacity of 1.2 mol salicylaldehyde per

DOI: 10.1021/ic503061z
Inorg. Chem. 2015, 54, 5169−5181

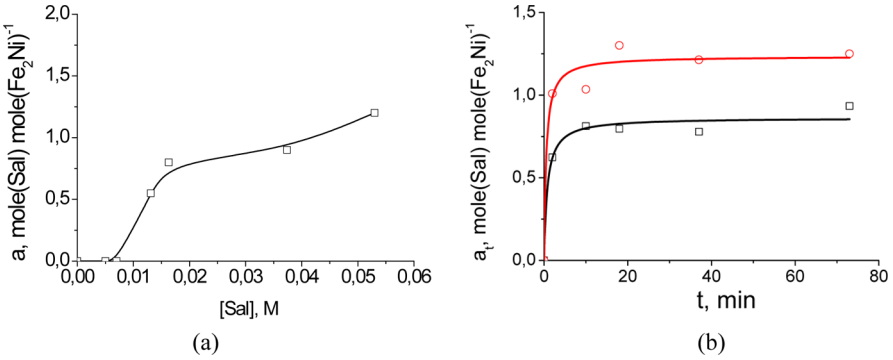

Figure 8. (a) Isotherm of salicylaldehyde sorption by **2** from toluene solution and (b) time dependence of salicylaldehyde sorption by **2** from toluene solution for $c(\mathrm{Sal})_0$ = 0.039 M (□) or $c(\mathrm{Sal})_0$ = 0.055 M (○). T = 373 K.

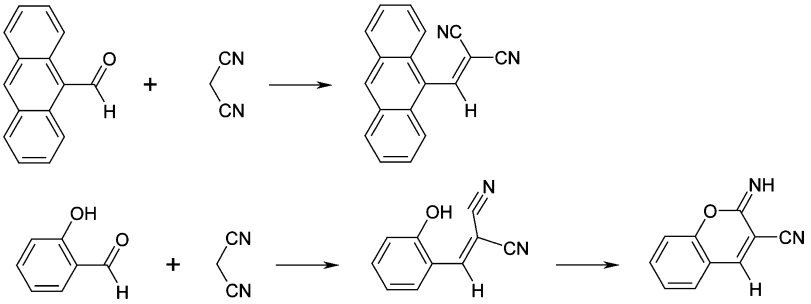

Figure 9. Condensation reactions of aldehydes with malononitrile catalyzed by **2**.

Fe_2Ni unit at $c(\mathrm{Sal})$ = 5.3 × 10^{-2} M. Estimation of salicylaldehyde sorption capacity, assuming that pores are filled by liquid salicylaldehyde at room temperature, gives the value corresponding to 3.1 molecules of salicylaldehyde per Fe_2Ni formula unit, indicating that the experimental data are consistent with partial filling of pores of **2** by salicylaldehyde. Notably, in contrast to salicylaldehyde sorption by **2**, isotherms of this aldehyde sorption by other MOFs under similar conditions were quite similar to those expected for type I, and the values of saturation sorption capacity were consistent with those expected for pore filling by liquid aldehyde.[43,44]

In addition, kinetics of salicylaldehyde sorption by **2** was studied (Figure 8b). The obtained data cannot be satisfactorily fit by a kinetic equation of the first order[45] or a mixed-sorption model,[45] thus indicating that sorption rate is not controlled by salicylaldehyde diffusion in pores. Application of the second-order equation[46] allowed us to fit the experimental data (Supporting Information Figure S13), giving k_2 = 0.38 mol(Fe_2Ni) mol(Sal)$^{-1}$ min^{-1} (average value for two different concentrations, details are presented in Supporting Information Figure S13). This value is significantly lower in comparison to sorption rate constants determined previously with the same pseudo-second-order model for salicylaldehyde sorption in Cu^{II} benzenetricarboxylate $[Cu_3(btc)_2]_n$, HKUST-1 (k_2 = 5.7 mol(Cu_2) mol(Sal)$^{-1}$ min^{-1} at 373 K),[44] or Fe^{III} benzenedicarboxylate $[Fe_2(OH)_{0.3}(H_2O)_{1.7}(btc)_{4/3}]Cl_{1.7}$ (k_2 = 4.3 mol(Fe_2) mol(Sal)$^{-1}$ min^{-1} at 373 K).[43] Besides, it is also much lower than the rate constant of xylenol orange adsorption in MIL-101(Cr) (3−90 mol(Cr_2) mol(XO)$^{-1}$ min^{-1}, depending on dye concentration, at T between 298 and 318 K).[47] Hence, the salicylaldehyde adsorption by **2** is much slower compared to that for similar systems, which can be explained by a smaller pore size or stronger competition between salicylaldehyde and solvent (toluene). Nevertheless, adsorption data do not contradict to the fact that pores of **2** are accessible to salicylaldehyde. In contrast, compound **2** does not adsorb 9-anthracenecarbaldehyde in similar conditions.

As mentioned above, catalytic activity of **2** was investigated in a condensation reaction between aldehydes and malononitrile. This process is typically catalyzed by coordination polymers containing basic[40] or acidic[48] sites, and in the case of **2** the noncoordinated N-atoms of triazine ring can be active catalytic sites. Condensation of aldehydes with malononitrile normally gives the derivative of 1,1-dicyanoethylene, which in the case of salicylaldehyde undergoes further intermolecular transformation to furnish 2-imino-2*H*-chromen-3-carbonitrile (Figure 9).[49] These reactions do not proceed without a catalyst, as confirmed by "blank experiments".

Reactions of malononitrile with salicylaldehyde or 9-anthracenecarbaldehyde in the presence of **2** gave expected products; no byproducts could be detected by ^{1}H NMR in the reaction mixtures. It was also shown previously that selectivity in this reaction is almost quantitative.[48] Thus, the values of aldehyde conversion correspond to the product yields (these were determined from spectra with respect to concentration of aldehyde, though equal initial concentrations of reagents were used). In the presence of **2**, the conversion of salicylaldehyde to condensation product, 2-imino-2*H*-chromen-3-carbonitrile, reaches 70% in 2 h. Then, the reaction rate decreases, and further heating of the reaction mixture for 38 h leads to just 18% increase of conversion (total conversion is 88%, Figure 10). In contrast, total conversion of 9-anthracenecarbaldehyde after 15 h of reaction is about 20%, increasing to 30% after 40 h of heating. Thus, the catalytic activity of **2** in the condensation of salicylaldehyde is much higher compared to that when using 9-anthracenecarbaldehyde as substrate. The conversions achieved with catalyst **2** in condensation of salicylaldehyde with malononitrile are comparable with those reported for a number

DOI: 10.1021/ic503061z
Inorg. Chem. 2015, 54, 5169−5181

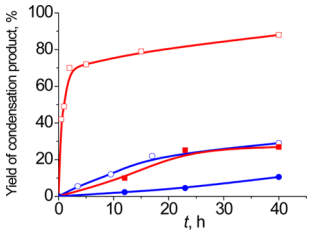

Figure 10. Time dependency of the condensation product yields for the reactions of salicylaldehyde (□ or ■) or 9-anthracenecarbaldehyde (○ or ●) with malononitrile catalyzed by **2** (red) or L^2 (blue). c(aldehyde) = 0.1 M, c(malononitrile) = 0.1 M, c(**2**) = $c(L^2)$ = 1.1 × 10^{-3} M (effective concentration), toluene, 100 °C.

of MOFs or polynuclear complexes in similar reactions. In addition, the activity of **2** in terms of catalyst turnover number (TON) exceeds the majority of reported catalysts[48,50−54] (Table S1, Supporting Information).

Considering the possibility of triazine moieties to catalyze such condensation reactions, we also performed control tests with L^2 as a catalyst instead of compound **2**. As in the case of **2**, reactions of salicylaldehyde or 9-anthracenecarbaldehyde with malononitrile in the presence of L^2 gave the same products, although in much lower yields under similar reaction conditions (e.g., 27% for L^2 vs 88% for **2** in the case of Sal substrate for the same catalyst loading and identical concentrations of the reagents, see also Figure 10). While the process involving **2** was heterogeneous, catalytic reaction in the presence of L^2 was partially homogeneous, but without achieving complete dissolution of L^2. Thus, higher activity of **2** compared to L^2 can be caused by better accessibility of the catalyst's active sites.

Conversion of salicylaldehyde in the presence of L^2 was 2−5 times higher compared to conversion of 9-anthracenecarbaldehyde, which can be explained by distinct reactivity of these aldehydes. However, there was 20-fold difference between conversions of these aldehydes at t = 2 h (or 10-fold at t = 5 h) in the case of catalysis by **2**. This value exceeds the difference in conversions associated with reactivity of aldehydes, and it can be explained by better accessibility of active sites of **2** to salicylaldehyde versus bulkier substrate (9-anthracenecarbaldehyde). The fact that the reaction of 9-anthracenecarbaldehyde occurs in the presence of **2** can provide evidence for the presence of some accessible active sites, located probably on the surface of microparticles of **2**. Apparently, these sites are active in catalytic condensations of both aldehydes, making the sieving effect (if any) less explicit. It should be noted that the substrate selectivity of **2** with respect to salicylaldehyde versus 9-anthracanecarbaldehyde was significantly higher than that for reported MOF $[Zr_6O_4(OH)_4(L^7)_6]_n$[52] (Supporting Information Table S1).

CONCLUSIONS

The present study has extended the growing family of coordination polymers built from the trimetallic hexacarboxylate $[M_3(\mu_3\text{-O})(\mu\text{-RCOO})_6]$ SBUs, resulting in the synthesis and characterization of the four new heterometallic Fe/Ni coordination polymers **2**, **3**, **4**, and **5**. These, along with the related derivatives **1** and **6**, have been topologically classified, revealing uninodal 3-connected underlying 2D, 1D, or 0D nets with distinct topologies. After additional simplification, these include the hcb (**1**, **2**), fes (**3**, **4**), SP 1-periodic net (4,4)(0,2) (**5**), and 3M8-1 (**6**) topologies constructed from the cluster $[Fe_2Ni(\mu_3\text{-O})(\mu\text{-Piv})_6]$ nodes and the polypyridine μ_3-$L^{1,2,3,4}$ or μ_2-$L^{5,6}$ blocks. The latter appear to play a crucial structure-driven role in defining the dimensionality and topological type of the resulting network.

In **2**, the values of pore volume found from N_2 sorption and sorption capacity regarding methanol and ethanol were close to those expected from the X-ray crystal structure. The isotherm of N_2 sorption by **2** resembled those of type I according to IUPAC classification, typical for microporous sorbents. The difference between sorption of methanol or ethanol by **2** was only in the shape of the isotherm (which can be explained by host−guest interaction energy), but not in the volume of pores accessible to these alcohols. In **2**, the volume of pores accessible to N_2, methanol, or ethanol was close to 0.3 $cm^3\ g^{-1}$, indicating that the pores could be completely filled by these substrates without any size discrimination. These findings point out that the crystal lattice of **2** is rigid and does not change upon interaction with N_2 and alcohols. Pores of **2** were accessible to salicylaldehyde, but the rate of its adsorption is rather low if compared to those of similar previously reported systems. Nevertheless, catalytic activity of **2** in the condensation of salicylaldehyde and malononitrile was significantly higher than its activity in a similar reaction involving 9-anthracenecarbaldehyde and malononitrile substrates. In addition, the difference between salicylaldehyde and 9-anthracenecarbaldehyde conversions catalyzed by **2** was higher than the corresponding difference in the reactions catalyzed by L^2. This finding can be partially explained by the sieving effect (discrimination of aldehyde molecules by size) rather than the higher reactivity of salicylaldehyde. Pore volumes for **3** and **3′** found from N_2 adsorption were much lower than the values expected from crystallographic data, which can be explained by pore blocking. Significant dependency of sorption characteristics of **3** on a sample's crystallinity (estimated from the width of reflections on powder XRD patterns) was found. It can be concluded that crystal lattice of **3** is less stable toward collapse than that of **2**.

The design of novel metal−organic materials constructed from the different heterometallic hexacarboxylate SBUs and polypyridine type spacers and the investigation of their functional properties are currently in progress.

ASSOCIATED CONTENT

Supporting Information

Additional characterization details, Figures S1−S11, Table S1 with comparison of catalytic activity, as well as CIF files for **2**−**5**. The Supporting Information is available free of charge on the ACS Publications website at DOI: 10.1021/ic503061z.

AUTHOR INFORMATION

Corresponding Authors

*E-mail: m_kiskin@mail.ru. Phone: +7(495)9522084. Fax: +7(495)9541279.

*E-mail: svk001@mail.ru. Phone: +38(044)5256661. Fax: +38(044)5256216.

Notes

The authors declare no competing financial interest.

ACKNOWLEDGMENTS

This work was partially supported by a joint grant of the National Academy of Sciences of Ukraine and Russian Foundation for Basic Research (No. 03-03-14), program of the National Academy of Sciences "Hydrogen in alternative energetics and novel technologies". A.M.K. acknowledges the

DOI: 10.1021/ic503061z
Inorg. Chem. 2015, 54, 5169−5181

Foundation for Science and Technology (FCT), Portugal (PTDC/QUI-QUI/121526/2010, PEst-OE/QUI/UI0100/2013). V.M.N. acknowledges the Russian Foundation for Basic Research (No. 14-03-90423). M.A.K. and I.L.E. acknowledge the Council on Grants of the President of the Russian Federation (Grants NSh-4773.2014.3).

REFERENCES

(1) (a) Gu, Z.-Y.; Yang, C.-X.; Chang, N.; Yan, X.-P. *Acc. Chem. Res.* **2012**, *45*, 734−745. (b) Chen, B.; Xiang, S.; Qian, G. *Acc. Chem. Res.* **2010**, *43*, 1115−1124. (c) Qiu, S.; Zhu, G. *Coord. Chem. Rev.* **2009**, *253*, 2891−2911. (d) Zhao, Z.; Ma, X.; Kasik, A.; Li, Z.; Lin, Y. S. *Ind. Eng. Chem. Res.* **2013**, *52*, 1102−1108. (e) Huang, K.; Liu, S.; Li, Q.; Jin, W. *Sep. Purif. Technol.* **2013**, *119*, 94−101. (f) Han, S.; Wei, Y.; Valente, C.; Lagzi, I.; Gassensmith, J. J.; Coskun, A.; Stoddart, J. F.; Grzybowski, B. A. *J. Am. Chem. Soc.* **2010**, *132*, 16358−16361. (g) Lu, H.; Zhu, S. *Eur. J. Inorg. Chem.* **2013**, 1294−1300. (h) Li, J.-R.; Sculley, J.; Zhou, H.-C. *Chem. Rev.* **2012**, *112*, 869−932. (i) Burtch, N. C.; Jasuja, H.; Walton, K. S. *Chem. Rev.* **2014**, *114*, 10575−10612.

(2) (a) Maihom, T.; Wannakao, S.; Boekfa, B.; Limtrakul, J. *J. Phys. Chem. C* **2013**, *117*, 17650−17658. (b) Wang, S.; Bromberg, L.; Schreuder-Gibson, H.; Hatton, T. A. *ACS Appl. Mater. Interfaces* **2013**, *5*, 1269−1278. (c) Fang, Q.-R.; Yuan, D.-Q.; Sculley, J.; Li, J.-R.; Han, Z.-B.; Zhou, H.-C. *Inorg. Chem.* **2010**, *49*, 11637−11642. (d) Kim, W.-S.; Lee, K. Y.; Ryu, E.-H.; Gu, J-M.; Kim, Y.; Lee, S. J.; Huh, S. *Eur. J. Inorg. Chem.* **2013**, 4228−4233. (e) Sen, R.; Saha, D.; Mal, D.; Brandão, P.; Lin, Z. *Eur. J. Inorg. Chem.* **2013**, 5103−5109. (f) Lee, J.; Farha, O. K.; Roberts, J.; Scheidt, K. A.; Nguyen, S. T.; Hupp, J. T. *Chem. Soc. Rev.* **2009**, *38*, 1450−1459. (g) Zhao, M.; Ou, S.; Wu, C.-D. *Acc. Chem. Res.* **2014**, *47*, 1199−1207. (h) Ou, S.; Wu, C.-D. *Inorg. Chem. Front.* **2014**, *1*, 721−734.

(3) (a) Suresh, P.; Radhakrishnan, S.; Babu, C. N.; Sathyanarayan, A.; Sampath, N.; Prabusankar, G. *Dalton Trans.* **2013**, *42*, 10838−10846. (b) Lestari, W. W.; Lönnecke, P.; Sárosi, M. B.; Streit, H. C.; Adlung, M.; Wickleder, C.; Handke, M.; Einicke, W.-D.; Gläserd, R.; Hey-Hawkins, E. *CrystEngComm* **2013**, *15*, 3874−3884. (c) Rao, X.; Song, T.; Gao, J.; Cui, Y.; Yang, Y.; Wu, C.; Chen, B.; Qian, G. *J. Am. Chem. Soc.* **2013**, *135*, 15559−15564. (d) Wanderley, M. M.; Wang, C.; Wu, C.-D.; Lin, W. *J. Am. Chem. Soc.* **2012**, *134*, 9050−9053.

(4) (a) Wriedt, M.; Yakovenko, A. A.; Halder, G. J.; Prosvirin, A. V.; Dunbar, K. R.; Zhou, H.-C. *J. Am. Chem. Soc.* **2013**, *135*, 4040−4050. (b) Maurice, R.; Verma, P.; Zadrozny, J. M.; Luo, S.; Borycz, J.; Long, J. R.; Truhlar, D. G.; Gagliardi, L. *Inorg. Chem* **2013**, *52*, 9379−9389. (c) Mohapatra, S.; Rajeswaran, B.; Chakraborty, A.; Sundaresan, A.; Maji, T. K. *Chem. Mater.* **2013**, *25*, 1673−1679.

(5) (a) Lan, A.; Li, K.; Wu, H.; Kong, L.; Nijem, N.; Olson, D. H.; Emge, T. J.; Chabal, Y. J.; Langreth, D. C.; Hong, M.; Li, J. *Inorg. Chem.* **2009**, *48*, 7165−7173. (b) Maspoch, D.; Ruiz-Molina, D.; Veciana, J. *Chem. Soc. Rev.* **2007**, *36*, 770−818. (c) Kolotilov, S. V.; Kiskin, M. A.; Eremenko, I. L.; Novotortsev, V. M. *Curr. Inorg. Chem.* **2013**, *3*, 144−160.

(6) (a) Robson, R. *Dalton Trans.* **2008**, 5113−5131. (b) Scherb, C.; Schödel, A.; Bein, T. *Angew. Chem., Int. Ed.* **2008**, *47*, 5777−5779. (c) Kim, H.; Das, S.; Kim, M. G.; Dybtsev, D. N.; Kim, Y.; Kim, K. *Inorg. Chem.* **2011**, *50*, 3691−3696. (d) Rosi, N. L.; Kim, J.; Eddaoudi, M.; Chen, B.; O'Keeffe, M.; Yaghi, O. M. *J. Am. Chem. Soc.* **2005**, *127*, 1504−1518.

(7) (a) Hong, K.; Bak, W.; Moon, D.; Chun, H. *Cryst. Growth Des.* **2013**, *13*, 4066−4070. (b) Vuong, G.-T.; Pham, M.-H.; Do, T.-O. *Dalton Trans.* **2013**, *42*, 550−557. (c) Perry, J. J., IV; Perman, J. A.; Zaworotko, M. J. *Chem. Soc. Rev.* **2009**, *38*, 1400−1417.

(8) Botezat, O.; van Leusen, J.; Kravtsov, V. Ch.; Filippova, I. G.; Hauser, J.; Speldrich, M.; Hermann, R. P.; Krämer, K. W.; Liu, S.-X.; Decurtins, S.; Kögerler, P.; Baca, S. G. *Cryst. Growth Des.* **2014**, *14*, 4721−4728.

(9) Dorofeeva, V. N.; Kolotilov, S. V.; Kiskin, M. A.; Polunin, R. A.; Dobrokhotova, Z. V.; Cador, O.; Golhen, S.; Ouahab, L.; Eremenko, I. L.; Novotortsev, V. M. *Chem. Eur. J.* **2012**, *18*, 5006−5012.

(10) Polunin, R. A.; Kolotilov, S. V.; Kiskin, M. A.; Cador, O.; Mikhalyova, E. A.; Lytvynenko, A. S.; Golhen, S.; Ouahab, L.; Ovcharenko, V. I.; Eremenko, I. L.; Novotortsev, V. M.; Pavlishchuk, V. V. *Eur. J. Inorg. Chem.* **2010**, 5055−5057.

(11) Polunin, R. A.; Kiskin, M. A.; Cador, O.; Kolotilov, S. V. *Inorg. Chim. Acta* **2012**, *380*, 201−210.

(12) Polunin, R. A.; Kolotilov, S. V.; Kiskin, M. A.; Cador, O.; Golhen, S.; Shvets, O. V.; Ouahab, L.; Dobrokhotova, Z. V.; Ovcharenko, V. I.; Eremenko, I. L.; Novotortsev, V. M.; Pavlishchuk, V. V. *Eur. J. Inorg. Chem.* **2011**, 4985−4992.

(13) (a) Schoedel, A.; Wojtas, L.; Kelley, S. P.; Rogers, R. D.; Eddaoudi, M.; Zaworotko, M. J. *Angew. Chem., Int. Ed.* **2011**, *50*, 11421−11424. (b) Dulcevscaia, G. M.; Filippova, I. G.; Speldrich, M.; van Leusen, J.; Kravtsov, V. Ch.; Baca, S. G.; Kögerler, P.; Liu, S.-X.; Decurtins, S. *Inorg. Chem.* **2012**, *51*, 5110−5117. (c) Pavlishchuk, A. V.; Kolotilov, S. V.; Zeller, M.; Thompson, L. K.; Addison, A. W. *Inorg. Chem.* **2014**, *53*, 1320−1330.

(14) (a) Deng, H.; Grunder, S.; Cordova, K. E.; Valente, C.; Furukawa, H.; Hmadeh, M.; Gándara, F.; Whalley, A. C.; Liu, Z.; Asahina, S.; Kazumori, H.; O'Keeffe, M.; Terasaki, O.; Stoddart, J. F.; Yaghi, O. M. *Science* **2012**, *336*, 1018−1023. (b) Deng, H.; Doonan, C. J.; Furukawa, H.; Ferreira, R. B.; Towne, J.; Knobler, C. B.; Wang, B.; Yaghi, O. M. *Science* **2010**, *327*, 846−850.

(15) (a) O'Keeffe, M. *Chem. Soc. Rev.* **2009**, *38*, 1215−1217. (b) O'Keeffe, M.; Peskov, M. A.; Ramsden, S. J.; Yaghi, O. M. *Acc. Chem. Res.* **2008**, *41*, 1782−1789. (c) Dybtsev, D. N.; Yutkin, M. P.; Peresypkina, E. V.; Virovets, A. V.; Serre, C.; Férey, G.; Fedin, V. P. *Inorg. Chem.* **2007**, *46*, 6843−6845. (d) Furukawa, H.; Go, Y. B.; Ko, N.; Park, Y. K.; Uribe-Romo, F. J.; Kim, J.; O'Keeffe, M.; Yaghi, O. M. *Inorg. Chem.* **2011**, *50*, 9147−9152.

(16) Shostakovskii, M. F.; Atavin, A. S.; Mirskova, A. N. *Zh. Obshch. Khim.* **1965**, *35*, 804−807.

(17) Barrios, L. A.; Ribas, J.; Aromí, G. *Inorg. Chem.* **2007**, *46*, 7154−7162.

(18) (a) Prikhod'ko, A.; Pointillart, F.; Golhen, S.; Gavrilenko, K. S.; Ouahab, L.; Kolotilov, S. V. *New J. Chem.* **2012**, *36*, 2070−2077. (b) Pauli, G. F.; Jaki, B. U.; Lankin, D. C. *J. Nat. Prod.* **2007**, *70*, 589−595. (c) Nuñez, A.; Hickner, M. A. *ACS Macro Lett.* **2013**, *2*, 49−52.

(19) Smith, C. B.; Raston, C. L.; Sobolev, A. N. *Green Chem.* **2005**, *7*, 650−654.

(20) *Bruker APEX2 Software Package*; Bruker AXS: Madison, WI, 2005.

(21) Sheldrick, G. M. *Acta Crystallogr.* **2008**, *A64*, 112−122.

(22) Sluis, P. v. d.; Spek, A. L. *Acta Crystallogr., Sect. A* **1990**, *46*, 194−201.

(23) Allampally, N. K.; Strassert, C. A.; Cola, L. D. *Dalton Trans.* **2012**, *41*, 13132−13137.

(24) Spek, A. L. *Acta Crystallogr., Sect. A* **1990**, *46*, c34.

(25) The values that characterize channel size in **1**, published in ref 9, did not take into account diameter of probe molecule, which should be added to the Mercury image.

(26) (a) Blatov, V. A. *IUCr Comp. Comm. Newsletter* **2006**, *7*, 4. (b) Blatov, V. A.; Shevchenko, A. P.; Proserpio, D. M. *Cryst. Growth Des.* **2014**, *14*, 3576−3586.

(27) (a) Blatov, V. A.; Proserpio, D. M. In *Modern Methods of Crystal Structure Prediction*; Oganov, A. R., Ed.; Wiley: New York, 2010; pp 1−28. (b) Blatov, V. A.; O'Keeffe, M.; Proserpio, D. M. *CrystEngComm* **2010**, *12*, 44. (c) Alexandrov, E. V.; Blatov, V. A.; Kochetkova, A. V.; Proserpio, D. M. *CrystEngComm* **2011**, *13*, 3947−3958.

(28) O'Keeffe, M.; Yaghi, O. M. *Chem. Rev.* **2012**, *112*, 675−702.

(29) For compounds with the 3,3,4L40 topology, see: (a) Zhang, Q.; Chung, I.; Jang, J. I.; Ketterson, J. B.; Kanatzidis, M. G. *Chem. Mater.* **2009**, *21*, 12−14. (b) Lytvynenko, A. S.; Kolotilov, S. V.; Cador, O.; Gavrilenko, K. S.; Golhen, S.; Ouahab, L.; Pavlishchuk, V. V. *Dalton Trans.* **2009**, 3503−3509. (c) Zheng, N.; Bu, X.; Feng, P. *Chem. Commun.* **2005**, 2805−2807. (d) Heller, M.; Sheldrick, W. S. *Z. Anorg. Allg. Chem.* **2004**, *630*, 1191−1195.

DOI: 10.1021/ic503061z
Inorg. Chem. 2015, 54, 5169−5181

(30) The Reticular Chemistry Structure Resource (RCSR) Database: O'Keeffe, M.; Peskov, M. A.; Ramsden, S. J.; Yaghi, O. M. *Acc. Chem. Res.* **2008**, *30*, 1782−1789.
(31) Mitina, T. G.; Blatov, V. A. *Cryst. Growth Des.* **2013**, *13*, 1655−1664.
(32) For recent examples of compounds with the fes topology, see: (a) Sun, J.-Y.; Wang, L.; Zhang, D.-J.; Li, D.; Cao, Y.; Zhang, L.-Y.; Zeng, S.-L.; Pang, G.-S.; Fan, Y.; Xu, J.-N.; Song, T.-Y. *CrystEngComm* **2013**, *15*, 3402−3411. (b) Li, D.-S.; Zhang, P.; Zhao, J.; Fang, Z.-F.; Du, M.; Zou, K.; Mu, Y.-Q. *Cryst. Growth Des.* **2012**, *12*, 1697−1702. (c) Gong, Y.; Wu, T.; Li, J.; Li, J. *Inorg. Chem. Commun.* **2012**, *19*, 39−42. (d) Wang, Y.-B.; Liu, D.-S.; Pan, T.-H.; Liang, Q.; Huang, X.-H.; Wu, S.-T.; Huang, C.-C. *CrystEngComm* **2010**, *12*, 3886−3893.
(33) See the Cambridge Structural Database (CSD, version 5.34, May 2013): Allen, F. H. *Acta Crystallogr.* **2002**, *B58*, 380−388.
(34) Kahr, J.; Mowat, J. P. S.; Slawin, A. M. Z.; Morris, R. E.; Fairen-Jimenez, D.; Wright, P. A. *Chem. Commun.* **2012**, *48*, 6690−6692.
(35) (a) Sing, K. S. W.; Everett, D. H.; Haul, R. A. W.; Moscou, L.; Pierotti, R. A.; Rouquerol, J.; Siemieniewska, T. *Pure Appl. Chem.* **1985**, *57*, 603−619. (b) Gregg, S. J.; Sing, K. S. W. In *Adsorption, Surface Area and Porosity*, 2nd ed.; Academic Press: London, 1982; p 4.
(36) Ross, S.; Olivier, J. P. *On Physical Adsorption*; Wiley and Sons: New York, 1964.
(37) Breck, D. W. *Zeolite Molecular Sieves*; Wiley-Interscience: New York, 1974.
(38) (a) Choi, S. B.; Furukawa, H.; Nam, H. J.; Jung, D.-Y.; Jhon, Y. H.; Walton, A.; Book, D.; O'Keeffe, M.; Yaghi, O. M.; Kim, J. *Angew. Chem.* **2012**, *124*, 8921−8925.
(39) (a) Sheveleva, A. M.; Kolokolov, D. I.; Gabrienko, A. A.; Stepanov, A. G.; Gromilov, S. A.; Shundrina, I. K.; Sagdeev, R. Z.; Fedin, M. V.; Bagryanskaya, E. G. *J. Phys. Chem. Lett.* **2014**, *5*, 20−24. (b) Kozachuk, O.; Meilikhov, M.; Yusenko, K.; Schneemann, A.; Jee, B.; Kuttatheyil, A. V.; Bertmer, M.; Sternemann, C.; Pöppl, A.; Fischer, R. A. *Eur. J. Inorg. Chem.* **2013**, *26*, 4546−4557.
(40) Fang, Q.-R.; Yuan, D.-Q.; Sculley, J.; Li, J.-R.; Han, Z.-B.; Zhou, H.-C. *Inorg. Chem.* **2010**, *49*, 11637−11642.
(41) Wolińska, E. *Tetrahedron* **2013**, *69*, 7269−7278.
(42) Gamez, P.; de Hoog, P.; Lutz, M.; Spek, A. L.; Reedijk, J. *Inorg. Chim. Acta* **2003**, *351*, 319−325.
(43) Sotnik, S. A.; Kolotilov, S. V.; Kiskin, M. A.; Dobrokhotova, Zh. V.; Gavrilenko, K. S.; Novotortsev, V. M.; Eremenko, I. L.; Imshennik, V. K.; Maksimov, Yu. V.; Pavlishchuk, V. V. *Russ. Chem. Bull.* **2014**, *4*, 862−869.
(44) Sotnik, S. A.; Gavrilenko, K. S.; Lytvynenko, A. S.; Kolotilov, S. V. *Inorg. Chim. Acta* **2015**, *426*, 119−125.
(45) Alosmanov, R. M. *Moscow Univ. Chem. Bull.* **2011**, *52*, 145−148.
(46) Wui, F.-C.; Tseng, R.-L.; Juang, R.-S. *Water Res.* **2001**, *35*, 613−618.
(47) Chen, C.; Zhang, M.; Guan, Q.; Li, W. *Chem. Eng. J.* **2012**, *183*, 60−67.
(48) Opanasenko, M.; Dhakshinamoorthy, A.; Shamzhy, M.; Nachtigall, P.; Horáček, M.; Garcia, H.; Čejka, J. *Catal. Sci. Technol.* **2013**, *3*, 500−507.
(49) (a) Deb, M. L.; Bhuyan, P. J. *Tetrahedron Lett.* **2005**, *46*, 6453−6456. (b) Karade, N. N.; Gampawar, S. V.; Shinde, S. V.; Jadhav, W. N. *Chin. J. Chem.* **2007**, *25*, 1686−1689.
(50) Liu, Y.; Zhang, R.; He, C.; Dang, D.; Duan, C. *Chem. Commun.* **2010**, *46*, 746−748.
(51) Wu, P.; Wang, J.; Li, Y.; He, C.; Xie, Z.; Duan, C. *Adv. Funct. Mater.* **2011**, *21*, 2788−2794.
(52) Yang, Y.; Yao, H.-F.; Xi, F.-G.; Gao, E.-Q. *J. Mol. Catal. A: Chem.* **2014**, *390*, 198−205.
(53) Murase, T.; Nishijima, Y.; Fujita, M. *J. Am. Chem. Soc.* **2012**, *134*, 162−164.
(54) Samanta, D.; Mukherjee, P. S. *Chem. Commum.* **2013**, *49*, 4307−4309.

DOI: 10.1021/ic503061z
Inorg. Chem. 2015, 54, 5169−5181